

# A Simplified State Interaction for Matrix Product State Wave Functions

Leon Freitag,<sup>\*,†</sup> Alberto Baiardi,<sup>‡</sup> Stefan Knecht,<sup>¶</sup> and Leticia González<sup>\*,†</sup>

<sup>†</sup>*Institute for Theoretical Chemistry, Faculty of Chemistry, University of Vienna,  
Währinger Str. 17, 1090 Vienna, Austria*

<sup>‡</sup>*ETH Zurich, Laboratory for Physical Chemistry, Vladimir-Prelog-Weg 2, 8093 Zurich,  
Switzerland*

<sup>¶</sup>*GSI Helmholtz Centre for Heavy Ion Research, Planckstr. 1, 64291 Darmstadt, Germany*

E-mail: leon.freitag@univie.ac.at; leticia.gonzalez@univie.ac.at

## Abstract

We present an approximation to the state-interaction approach for matrix product state (MPS) wave functions (MPSSI) in a non-orthogonal molecular orbital basis, first presented by Knecht et al. [J. Chem. Theory Comput., 2016, 28, 5881], that allows for a significant reduction of the computational cost without significantly compromising its accuracy. The approximation is well-suited if the molecular orbital basis is close to orthogonality, and its reliability may be estimated a-priori with a single numerical parameter. For an example of a platinum azide complex, our approximation offers up to 63-fold reduction in computational time compared to the original method for wave-function overlaps and spin-orbit couplings, while still maintaining numerical accuracy.

# 1 Introduction

Accurate calculations of many photochemical processes can be a daunting task. Excited state are often governed by strong electron correlation effects and many close-lying excited states, where multiconfigurational electronic structure methods<sup>1,2</sup> are indispensable.

Multiconfigurational methods based on the complete active space self-consistent-field (CASSCF)<sup>3</sup> are well established for handling strong correlation effects. These approaches require selecting an orbital subspace called *active orbital space* whose size determines the computational cost. Traditional CASSCF methods scale exponentially with the number of the active orbitals and electrons, allowing for calculations of up to 22 electrons in 22 orbitals with a massively parallel approach,<sup>4</sup> but limiting its size to approximately 18 electrons in 18 orbitals<sup>5</sup> under more moderate computational time requirements. These limits can be reached very quickly, especially in polynuclear transition metal complexes. One approach to overcome the exponential scaling of CASSCF is the density matrix renormalisation group (DMRG)<sup>6,7</sup> for quantum chemistry,<sup>8-16</sup> which, combined with self-consistent field orbital optimisation (DMRG-SCF)<sup>17,18</sup> is able to variationally approximate CASSCF wavefunctions to arbitrary accuracy at a polynomial instead of exponential scaling of the computational cost.

In the CASSCF paradigm, and also with DMRG-SCF, excited states are usually calculated with a *state-average* ansatz, where a single orthonormal set of molecular orbitals (MOs) is optimised to provide a balanced representation of several states. This allows for a straightforward calculation of transition densities and moments that are required to compute properties such as oscillator strengths, magnetic properties or spin-orbit couplings. However, state-averaging is not always possible or desired: (i) the individual state characters differ too much for an average set of orbitals to yield an adequate description; (ii) state-averaging e.g. between different spin multiplicities is not supported by the computer implementation of the method, or (iii) a single molecular set of orbitals is simply not possible at all because, for example, the states in question belong to different molecular structures. In such cases,

each state is optimized independently and the resulting MO bases for the individual states are no longer the same. As a consequence, the states are no longer mutually orthogonal, turning the calculation of transition densities and moments into a challenging task.

A solution to this predicament is to use the *complete active space state interaction* (CASSI) method, proposed by Malmqvist and Roos,<sup>19,20</sup> who suggested to transform the MO bases for the individual states to a biorthonormal basis. Along with the orbital rotation, this requires a simultaneous “counter-rotation” of the wavefunction expansion coefficients: for a configuration interaction (CI)-type wavefunctions, which include CASSCF wavefunctions, this step can be achieved with a series of single-orbital transformations.<sup>20,21</sup> After transformation to biorthonormal basis, wavefunction overlaps and transition densities may be evaluated at little to no computational overhead.

The CASSI approach was soon extended to calculate spin-orbit couplings,<sup>22</sup> and with the advent of DMRG for quantum chemistry, the DMRG-based version of CASSI, later named the *matrix product state state interaction* (sic!) (MPSSI) has been introduced.<sup>23</sup> To account for spin-orbit interaction with DMRG wavefunctions, several other approaches based on spin-free wavefunctions that share a *common* MO basis were developed<sup>24–26</sup> as well as a fully-relativistic four-component approach<sup>27,28</sup>.

Multiconfigurational methods and, specifically, the CASSCF method, are often used as an underlying method for the electronic structure calculations for ab-initio nonadiabatic dynamics:<sup>29</sup> partially due to its computational efficiency for small systems and ability to describe strong correlation, but also because of the readily-available implementations for gradients and non-adiabatic couplings.<sup>30–33</sup> With the help of the CASSI method, ab-initio nonadiabatic excited state dynamics with spin-orbit couplings, e. g. with the SHARC approach<sup>34</sup> may be employed to study processes involving different spin states coupled via intersystem crossing. Additionally, overlaps between wavefunctions at different time steps may also be calculated with CASSI and may serve to approximate non-adiabatic couplings that are included in the on-the-fly propagation of nuclear wavefunctions.<sup>35</sup> The steep scaling of CASSCF with re-

spect to the active orbital space may be tamed with DMRG-SCF also with surface-hopping dynamics, as the calculation of the analytical gradients and nonadiabatic couplings has been recently reported,<sup>36</sup> and spin-orbit couplings and wavefunction overlaps may be calculated with MPSSI. DMRG-SCF, despite its polynomial scaling of the computational time with the active space size, is, nevertheless computationally very intensive, and MPSSI is also a cost-intensive method with a computational cost comparable to that of DMRG-SCF. Dynamics calculations, however, require a cheap and performant electronic structure method, as electronic structure calculations of energies, gradients and couplings are carried out for hundreds or thousands of time steps. Accordingly, elimination of every possible bottleneck in the electronic structure calculations is extremely beneficial for dynamics calculations.

In this work, we identify and address the bottlenecks of the MPSSI approach, allowing us to significantly improve its performance by introducing two approximations, whose accuracy can easily be assessed based on a single parameter. We demonstrate the effectiveness of these approximations by means of MPSSI calculations of wavefunction overlaps and spin-orbit couplings for a medium-sized transition metal complex.

## 2 Theory

As the starting points of this work, we first outline the CASSI and the MPSSI approaches. Assume two sets of multiconfigurational wave functions  $|\Psi^X\rangle$  and  $|\Psi^Y\rangle$ , each expressed in their own MO basis  $\{\phi_p^X\}$  and  $\{\phi_p^Y\}$ , respectively, which are not mutually orthogonal. The goal of the CASSI approach is to find the biorthonormal MO bases  $\{\phi_p^A\}$  and  $\{\phi_p^B\}$ , such that

$$\langle \phi_p^A | \phi_q^B \rangle = \delta_{pq} \tag{1}$$

and a corresponding transformation of the wavefunctions  $|\Psi^X\rangle$  and  $|\Psi^Y\rangle$ , such that the transition matrix elements  $\langle \Psi^X | \hat{\mathcal{O}} | \Psi^Y \rangle_{pq}$  of any operator  $\hat{\mathcal{O}}$  may be calculated with very little additional computational effort compared to the case where  $|\Psi^X\rangle$  and  $|\Psi^Y\rangle$  belong to

the same MO basis. To this end,<sup>20</sup> an LU decomposition of the inverse of the orbital overlap matrix  $\mathbf{S}^{\text{XY}}$  (with  $S_{pq}^{\text{XY}} = \langle \phi_p^{\text{X}} | \phi_q^{\text{Y}} \rangle$ ) is constructed:

$$(\mathbf{S}^{\text{XY}})^{-1} = \mathbf{C}^{\text{XA}} (\mathbf{C}^{\text{YB}})^\dagger \quad (2)$$

The  $\mathbf{C}^{\text{XA}}$  and  $\mathbf{C}^{\text{YB}}$  matrices define the transformation from the MO to the biorthogonal basis, such that

$$\phi^{\text{A}} = \phi^{\text{X}} \mathbf{C}^{\text{XA}}; \quad \phi^{\text{B}} = \phi^{\text{Y}} \mathbf{C}^{\text{YB}}. \quad (3)$$

Before proceeding to the transformation of the wave functions  $|\Psi^{\text{X}}\rangle$ , let us briefly introduce the wave function ansatz employed with DMRG, the *matrix product states*. A general CI ansatz for an arbitrary wave function  $|\Psi\rangle$  in a Hilbert space spanned by  $L$  spatial orbitals may be expressed as

$$|\Psi\rangle = \sum_{k_1 \dots k_L} c_{k_1 \dots k_L} |k_1 \dots k_L\rangle \quad (4)$$

with  $c_{k_1 \dots k_L}$  as the CI coefficients and  $|k_1 \dots k_L\rangle$  as occupation number vectors. The notation  $|k_1 \dots k_L\rangle$  reflects the fact that for each spatial orbital  $l$  we may have a local basis state  $|k_l\rangle = \{|\uparrow\downarrow\rangle, |\uparrow\rangle, |\downarrow\rangle, |0\rangle\}$  and the total occupation number vector consists of local occupations of all orbitals  $1, \dots, L$ .

The CI coefficients  $c_{k_1, \dots, k_L}$  may be reshaped as an  $L$ -dimensional tensor and decomposed<sup>37,38</sup> by repeated application of the singular value decomposition into a product of matrices  $\mathbf{M}^{k_l}$ , yielding a *matrix product state* (MPS):

$$|\Psi\rangle = \sum_{k_1 \dots k_L} \sum_{a_1 \dots a_{L-1}} M_{1a_1}^{k_1} M_{a_1 a_2}^{k_2} \dots M_{a_{L-1} 1}^{k_L} |k_1 \dots k_L\rangle \quad (5)$$

The dimension of matrices (i. e. the  $a$  indices) may be limited to a certain maximum dimension  $m$ , usually referred to as *number of renormalised block states* or *maximum bond dimension*. This way, the number of parameters entering the wave function *ansatz* definition is reduced from exponential, as it is in full CI, to polynomial. The optimisation of MPS

wave functions is most commonly carried out with the DMRG approach, for the explanation of which we refer the reader to the comprehensive reviews of Schollwöck<sup>37,38</sup> and Ref. 16.

Analogously to the MPS, operators may be expressed in a *matrix product operator* (MPO) form as,

$$\hat{\mathcal{W}} = \sum_{k,k'} \sum_{b_1 \dots b_{L-1}} W_{1b_1}^{k_1 k'_1} W_{b_1 b_2}^{k_2 k'_2} \dots W_{b_{L-1} 1}^{k_L k'_L} |k_1 \dots k_L\rangle \langle k_1 \dots k_L| \quad (6)$$

We consider next the transformation algorithm for wave functions  $|\Psi^X\rangle$ , when  $|\Psi^X\rangle$  are MPS, as introduced in Ref. 23. We perform another LU decomposition, this time of the  $\mathbf{C}^{\text{XA}}$  matrix, and from its lower- and upper triangular parts ( $\mathbf{C}_L^{\text{XA}}$  and  $\mathbf{C}_U^{\text{XA}}$ , respectively), we construct the matrix  $\mathbf{t}$ , with its lower and upper triangular part being

$$\mathbf{t}_U = (\mathbf{C}_U^{\text{XA}})^{-1} \quad (7)$$

$$\mathbf{t}_L = 1 - \mathbf{C}_L^{\text{XA}}. \quad (8)$$

The matrix  $\mathbf{t}$  is then used to transform the wave functions  $|\Psi^X\rangle$  as follows:

- First, the inactive orbitals are transformed by scaling the MPS with a factor  $\alpha$  given by

$$\alpha = \prod_{i=1}^{n_I} t_{ii}^2, \quad (9)$$

where  $i$  runs over all inactive orbitals.

- For the subsequent transformation with respect to the *active* orbitals, the following steps are repeated for each active orbital  $l$ :

- i) Each matrix  $\mathbf{M}^{k_l}$  is multiplied with  $t_{ll}^2$  for  $k_l = |\uparrow\downarrow\rangle$  and with  $t_{ll}$  for  $k_l = |\uparrow\rangle$  and  $|\downarrow\rangle$ ,

ii) an MPO  $\hat{\mathcal{W}}$  is applied to the scaled MPS  $|\tilde{\Psi}^X\rangle$  yielding a transformed MPS

$$|\tilde{\Psi}^A\rangle = \hat{\mathcal{W}}|\tilde{\Psi}^X\rangle \quad (10)$$

with

$$\hat{\mathcal{W}} = \left( \hat{1} + \hat{\mathcal{T}} + \frac{1}{2}\hat{\mathcal{T}}^2 \right) \quad (11)$$

and

$$\hat{\mathcal{T}} = \sum_{m \neq j}^L \frac{t_{mj}}{t_{jj}} \left( a_{m\uparrow}^\dagger a_{j\uparrow} + a_{m\downarrow}^\dagger a_{j\downarrow} \right). \quad (12)$$

iii) In the last step, one performs an SVD compression of  $|\tilde{\Psi}^A\rangle$  to obtain the final MPS  $|\Psi^A\rangle$ , a representation of the original state in the biorthonormal basis  $\{\phi^A\}$ . Analogously,  $|\Psi^B\rangle$  may be constructed by repeating the steps above with the  $\mathbf{C}^{YB}$  matrix and  $|\Psi^Y\rangle$  MPS.  $|\Psi^A\rangle$  and  $|\Psi^B\rangle$  are then employed to calculate transition density matrix elements and properties.

While the original MPS transformation algorithm (MPSSI) as been shown to be highly accurate for various properties, including spin-orbit couplings and g-factors of actinides,<sup>23</sup> its current implementation has two major bottlenecks.

The first bottleneck originates from the SVD compression from step iii): the application of the MPO in Eq. (10) to an MPS results in a transformed MPS with the maximum bond dimension of  $b \times m$ , where  $b$  is the maximum bond dimension of the MPO  $\hat{\mathcal{W}}$  and  $m$  the maximum bond dimension of MPS  $|\tilde{\Psi}^X\rangle$ . The final SVD compression in step iii) reduces the final bond dimension of the transformed MPS, which is necessary since the storage size of the MPS and the cost of transition density matrix element evaluation<sup>39</sup> scales with  $\mathcal{O}(m^2L)$ , and thus becomes prohibitively expensive for large  $m$ . However, MPS compression itself is a computationally expensive step with a computational cost of  $\mathcal{O}(m^3L)$ , and constitutes a crucial bottleneck in MPSSI. The original MPSSI implementation<sup>23</sup> employs a fixed value of  $m = 8000$ , preserving the expectation value of the energy up to  $10^{-8}$  a. u., but at a price

of significant computational cost.

The second bottleneck arises from the construction of the  $\hat{\mathcal{W}}$  MPO: as shown in Eq. (11), this step requires the construction of the  $\hat{\mathcal{T}}^2$  operator, which is not trivial. The original implementation<sup>23</sup> avoids this problem by calculating  $\hat{\mathcal{T}}|\tilde{\Psi}^X\rangle$  and  $\hat{\mathcal{T}}(\hat{\mathcal{T}}|\tilde{\Psi}^X\rangle)$  and adding the resulting MPS afterwards. Applying the  $\hat{\mathcal{T}}$  operator twice, however, increases the bond dimension of the resulting MPS by a factor of  $b^2$  and requires an additional MPS compression step between the first and the second application of  $\hat{\mathcal{T}}$ .

In this work we improve the efficiency of the MPSSI method by introducing two simple but effective changes to the MPS transformation algorithm. The first is the first-order approximation of Eq. (11) by neglecting the final second-order term. This approximation may be justified as follows: since to allow for the formation of biorthogonal bases the original MO bases have to be sufficiently similar, i.e. show an overlap fairly close to unity, the resulting  $\mathbf{t}$  matrix should not deviate significantly from the identity matrix. Eq. (11) can be clearly recognised as a second-order Taylor approximation to the exponential of  $\hat{\mathcal{T}}$ , and in the regime of  $\mathbf{t}$  close to identity also the linear approximation should hold. In addition, Eq. (12) shows that the  $\hat{\mathcal{T}}$  operator is scaled with the ratio between the off-diagonal and diagonal elements of  $\mathbf{t}$ . For an orthogonal basis,  $\mathbf{t}$  will be the identity matrix and this ratio will be zero. Therefore, a simple estimate based on off-diagonal elements of  $\mathbf{t}$ , such as the  $L^2$  norm of  $\mathbf{t} - \mathbf{I}_L$  (with  $\mathbf{I}_L$  as an  $L \times L$  identity matrix) may be employed as a measure of the accuracy of the approximation.

The second approximation is the reduction of the maximum bond dimension of the compressed MPS, therefore reducing the computational cost of the MPS compression.

In the following section we demonstrate that both approaches significantly improve the computational cost of MPSSI with almost no effect on accuracy. Although both steps reduce the accuracy of the transformation, the following numerical test demonstrate that the errors introduced are negligible for several types of properties.

### 3 Numerical Examples

As a testbed we employ *trans,trans,trans*-[Pt(N<sub>3</sub>)<sub>2</sub>(OH)<sub>2</sub>(NH<sub>3</sub>)<sub>2</sub>] (in the following referred to as **1**), which is a flagship Pt(IV) azide complex, relevant in photoactivated cancer chemotherapy.<sup>40–42</sup> As the majority of 5d metal compounds, **1** shows strong spin-orbit couplings and since its photoactivation mechanism involves azide dissociation, such process is best described by multiconfigurational methods.<sup>43</sup>

**Performance of MPSSI approximation on wavefunction overlaps.** In principle, CASSI/MPSSI allow for an easy calculation of wavefunction overlaps constructed with nonorthogonal orbital sets. Wavefunction overlaps, especially between states at different molecular structures or spin multiplicities, are widely used in ab-initio excited state molecular dynamics<sup>35,44–46</sup> or in wavefunction analysis.<sup>47</sup> Here we investigated the goodness of the linear approximation to  $\hat{\mathcal{W}}$  (in the following called as “MPSSI approximation”) for wavefunction overlaps of both ground and excited states for varying molecular structures of the same molecule. With an increasing deviation of molecular structures, the dissimilarity of the orbitals and the  $L^2$  norm of the  $\|\mathbf{t} - \mathbf{I}_L\|$  matrix also increases, allowing us to assess also the limits of the MPSSI approximation with the increasing norm.

We performed CASSCF and DMRG-SCF calculations with a comparably small active space of 8 electrons in 9 orbitals. This active space is capable to qualitatively describe the energies of the lowest excited states, and is also small enough for DMRG-SCF to be able to reproduce the CASSCF results almost exactly: the final DMRG-SCF energies differ from their CASSCF counterparts by no more than  $10^{-7}$  a. u.

We performed a rigid scan along the Pt–N bond of one of the azide ligands with CASSCF and DMRG-SCF, and calculated the wavefunction overlap of the lowest five singlet states at structures with an elongated Pt–N bond with their counterparts at the equilibrium structure. We calculated the overlaps of the CASSCF wavefunctions with CASSI, those of DMRG-SCF wavefunctions with full and approximate MPSSI: the average pairwise differences between

these are shown in Fig. 1a. The overlap difference between CASSCF and full MPSSI (green line) reflects the error arising only due to DMRG approximation to the CASSCF wavefunction. The effect arising due to the MPSSI approximation can be fully estimated from the approximate to full MPSSI difference (red line). The corresponding changes in the  $L^2$  norm of  $\mathbf{t} - \mathbf{I}_L$  matrices are shown in Fig. 1b.

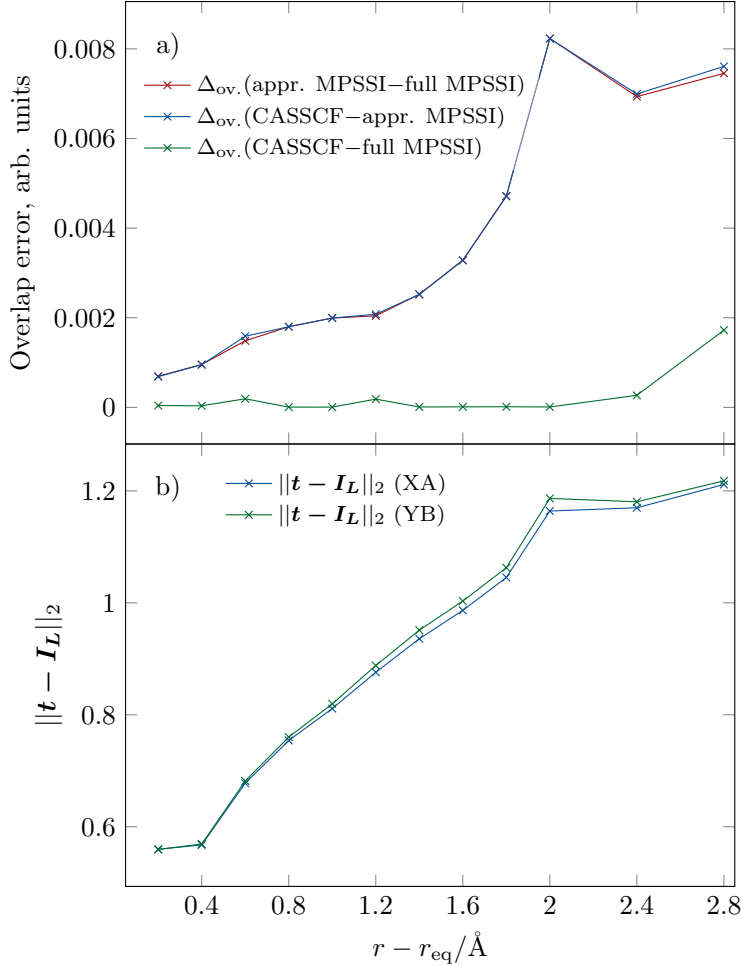


Figure 1: (a) Average differences of overlaps calculated with CASSCF, full and approximate MPSSI; (b)  $L_2$  norm of  $\mathbf{t} - \mathbf{I}_L$  matrices, with  $\mathbf{I}_L$  as the identity matrix; XA corresponds to the orbitals at the equilibrium structure, YB to orbitals at a given  $r - r_{\text{eq}}$ .

Given the tightly-converged DMRG-SCF wavefunction, the errors arising due to the DMRG approximation are negligible: for all  $r - r_{\text{eq}}$  values except  $2.8 \text{ \AA}$  the overlap error is less than  $3 \times 10^{-4}$ , whereas for the latter calculation it rises slightly to  $2 \times 10^{-3}$ . This discrepancy is due to a slightly poorer convergence of the wavefunction at this particular  $r - r_{\text{eq}}$  value

than for other Pt–N bond lengths. Recalling that, in contrast to the quadratic convergence of the energy, property calculations converge linearly with respect to the wavefunction quality, the maximum energy error for this case is closer to  $10^{-7}$  a. u., whereas for other Pt–N bond lengths it is well below this value. Nevertheless, all of these errors are so small they may be considered negligible. The MPSSI approximation error is however larger than the DMRG approximation error for all calculations, and rises with increasing  $\mathbf{t} - \mathbf{I}_L$  norm: starting with approximately  $4 \times 10^{-4}$  at  $r - r_{\text{eq}} = 0.2 \text{ \AA}$  with a corresponding  $\mathbf{t} - \mathbf{I}_L$  norm of 0.4 (and thus remaining in the same order of magnitude as the DMRG approximation errors), it steadily increases with increasing  $\mathbf{t} - \mathbf{I}_L$  norm, reaching values of  $8 \times 10^{-3}$  for the extended Pt–N bonds.

In the range of  $r - r_{\text{eq}}$  of  $1.2 \text{ \AA}$  to  $1.8 \text{ \AA}$  we see a particularly large increase of the MPSSI approximation error, which corresponds to  $\mathbf{t} - \mathbf{I}_L$  norm values of 0.9 to 1. Therefore, we propose a conservative cut-off  $\mathbf{t} - \mathbf{I}_L$  norm value of 1, below which we recommend to use the approximation. This choice is, however, largely arbitrary: the average overlap error at the cutoff value is  $2 \times 10^{-3}$ , and even the largest error value of  $8 \times 10^{-3}$  in these calculation series is still sufficient for a qualitatively correct calculation.

The suitability of larger MPSSI approximation errors for qualitative calculations is best illustrated if one compares the results to those from a partially-converged DMRG-SCF calculation, which is a common practice in the literature. Figure 2 shows the same overlap errors displayed in Fig. 1a but for partially converged DMRG-SCF wavefunctions, where energy differences to the corresponding CASSCF wavefunction are up to  $2 \times 10^{-4}$  a. u. The norms of the  $\mathbf{t} - \mathbf{I}_L$  matrices are similar and the MPSSI approximation errors are almost the same as the corresponding errors for the fully-converged DMRG-SCF wavefunctions. However, the errors arising due to the DMRG approximation increase sharply with the decreasing DMRG-SCF wavefunction quality. For energy errors in the range of  $10^{-4}$  a. u. to  $10^{-5}$  a. u., typical for large-scale DMRG calculations, the order of magnitude of the MPSSI approximation and the DMRG approximation error is similar, and therefore approximate MPSSI is still suitable

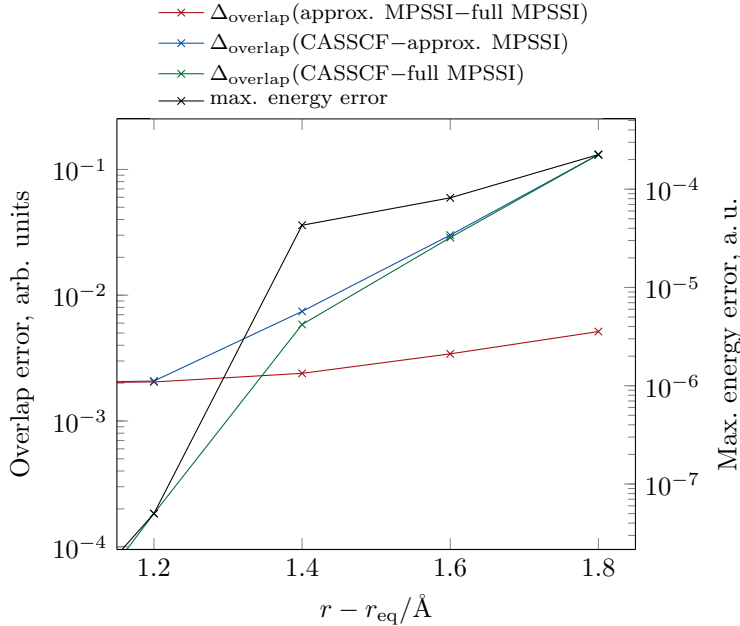


Figure 2: Average overlap error for overlaps with CASSCF, full and approximate MPSSI, for a partially-converged DMRG-SCF wavefunction. Maximum energy error with respect to a corresponding CASSCF calculation is shown in black.

for qualitative calculations.

We may conclude that the MPSSI approximation error is independent of the DMRG wavefunction quality but rather depends only on the  $\mathbf{t}$  matrix. Thus, the  $L^2$  norm of the  $\mathbf{t} - \mathbf{I}_L$  matrix constitutes an easy metric available prior to the MPSSI rotation, that allows a simple decision whether the MPSSI approximation should be employed or not.

**Performance of MPSSI approximation on spin-orbit couplings.** Here we investigate the MPSSI approximation performance in the calculation of spin-orbit coupling matrix elements, which is another typical use case for MPSSI. We employ the same active space of 8 electrons in 9 orbitals as in the previous example, but calculate energies and spin-orbit coupling matrix elements for the five lowest singlets and triplet states of  $\mathbf{1}$  at the equilibrium structure.

Figure 3a shows spin-orbit couplings calculated with CASSCF, DMRG-SCF employing the original (full)-,<sup>23</sup> and the approximate MPSSI scheme. As in the previous example,

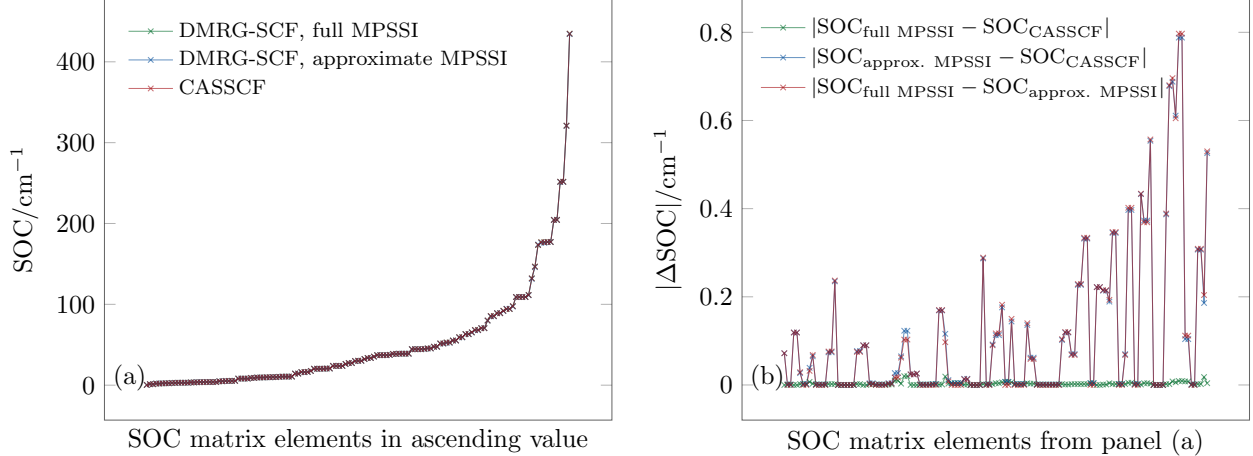


Figure 3: (a) Spin-orbit coupling (SOC) matrix elements for the first 5 singlet and 5 triplet states at the equilibrium structure of **1** for an active space of 8 electrons in 9 orbitals. (b) Absolute errors of the SOC matrix elements in panel (a).

DMRG-SCF wavefunctions have been converged so that the DMRG-SCF energies differ from their CASSCF counterparts by less than  $10^{-7}$  a. u.: therefore any error arising from the DMRG approximation is negligible. The differences between the calculated values are displayed in Figure 3b and show that the effect of the DMRG approximation (green curve) is indeed negligible: the largest error due to the DMRG approximation does not exceed  $0.02 \text{ cm}^{-1}$ . The error due to the MPSSI approximation is, similarly to the previous example, slightly larger, but still negligible for all practical purposes: the average error is  $0.077 \text{ cm}^{-1}$  and the maximum error is approximately  $0.8 \text{ cm}^{-1}$ .

As in the previous example, we also consider the case of a partially-converged DMRG-SCF wavefunction, where the energies of some states differ up to  $10^{-5}$  a. u. from their CASSCF counterparts. This accuracy is typical for large-scale DMRG-SCF calculations and is more than sufficient for accurate absorption energies up to  $10^{-5}$  a. u. The results are displayed in Figure 4. We note that in this case the SOC error arising from the DMRG-SCF approximation increases by several orders of magnitude up to  $30 \text{ cm}^{-1}$ , while the MPSSI approximation error remains the same. Thus, in this case the total error in the DMRG calculation largely consists of the DMRG approximation error while the MPSSI approximation error is completely negligible.

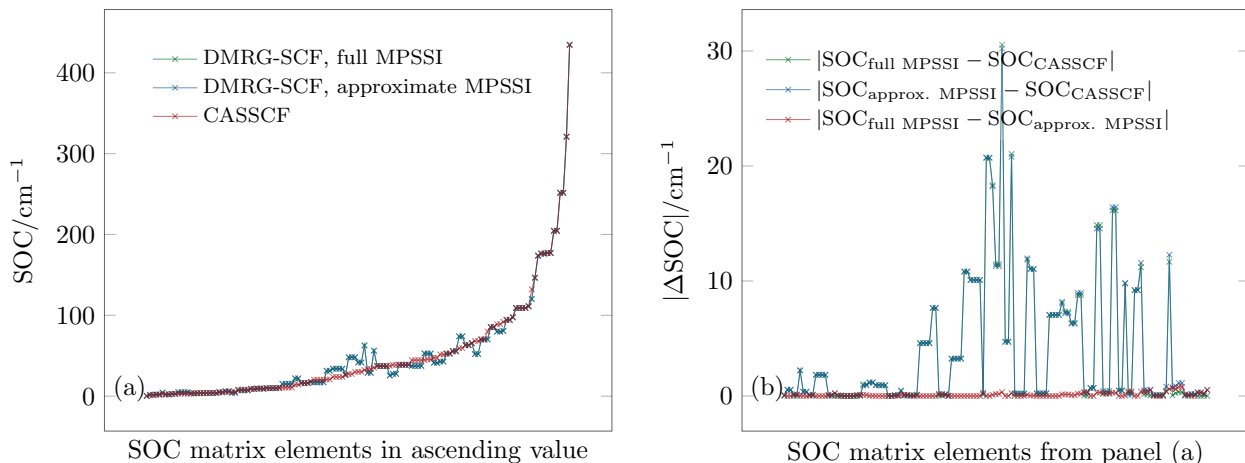


Figure 4: (a) Spin-orbit coupling (SOC) matrix elements for the first 5 singlet and 5 triplet states at the equilibrium structure of **1** with a partially-converged DMRG-SCF wavefunction (b) Absolute errors of the SOC matrix elements in panel (a).

Finally, we would like to mention the computational time savings arising from the approximation. Due to the small size of the active space, the MPSSI approximation is not the bottleneck in this calculation, but it already reduces the computational time by approximately 40%, i. e. from 10 min 7 s to 6 min 6 s of run time on 4 cores of an Intel Xeon E5-2650 CPU.

**Performance of the methods with a larger active space.** From a calculation using time-dependent density functional theory (TD-DFT, CAM-B3LYP/def2-TZVPP) and including several low-lying singlet excited states of **1**, we know that CASSCF and DMRG-SCF calculations with an active space of 8 electrons in 9 orbitals, as employed in the previous section, cannot even qualitatively account for the spin-orbit couplings: the largest absolute value for the spin-orbit coupling between five lowest singlet and triplet excited states was  $434 \text{ cm}^{-1}$ , whereas an analogous value from the TD-DFT calculation was found to be approximately  $1800 \text{ cm}^{-1}$ .

This insufficiency can be remedied by a DMRG-SCF calculation with 26 electrons in 19 orbitals, as employed in Ref. 43. As this active space is computationally too expensive for a CASSCF calculation, only DMRG-SCF calculations with subsequent approximate and full

MPSSI calculations are performed. In addition, we assess the error arising due to the MPS compression step in the MPS transformation by testing various  $m$  values for the compressed MPS: the DMRG-SCF calculations were performed for  $m = 500$ , but during the MPSSI procedure the intermediate MPS during rotation was compressed either to the original  $m = 500$ , or to  $m = 2000$ . Note that we could not afford a post-compression  $m$  value of 8000 from the original paper of Knecht et al.<sup>23</sup> due to its prohibitive computational requirements. Furthermore, in the following we consider the 10 lowest singlet and 9 triplet states. The calculated SOC and their errors are shown in Fig. 5.

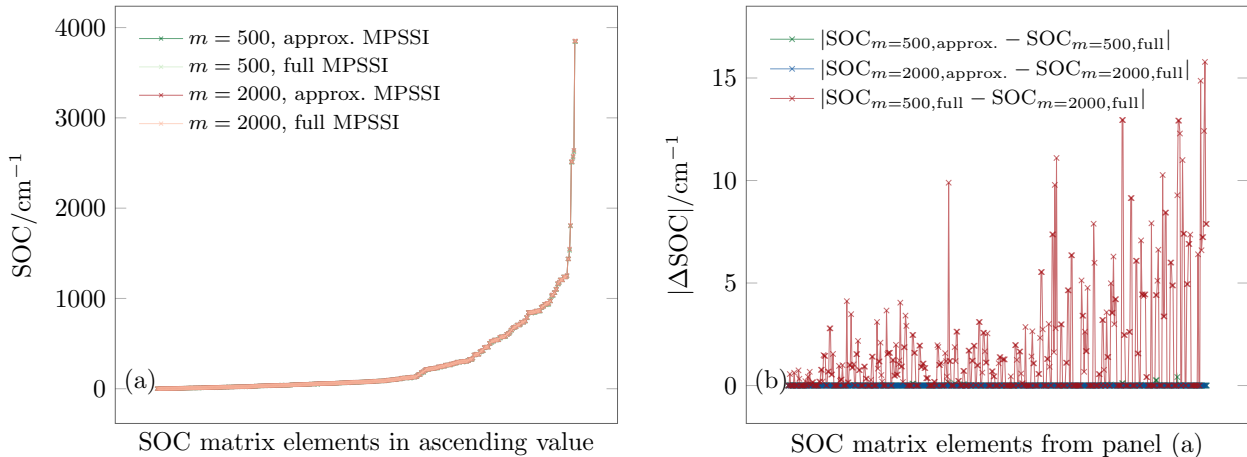


Figure 5: (a) Spin-orbit coupling (SOC) matrix elements for the first 10 singlet and 9 triplet states at the equilibrium structure of **1**, for an active space of 26 electrons in 19 orbitals. (b) Absolute errors of the SOC matrix elements in panel (a).

As can be seen from Fig. 5a, all methods yield almost identical values for the SOC. A closer look at errors (Fig. 5b) reveals a maximum error of approximately  $15 \text{ cm}^{-1}$ , which arises entirely due to the MPS compression. The MPSSI approximation error is negligible: the maximum MPSSI approximation error is  $0.41 \text{ cm}^{-1}$  for  $m = 500$  and just  $1 \times 10^{-3} \text{ cm}^{-1}$  for  $m = 2000$ . The small MPSSI approximation error is not surprising for this calculation, as the  $\mathbf{t} - \mathbf{I}_L$  norms are only 0.002 and 0.006. We can also see that the MPSSI approximation is affected by compression, but only very slightly: it is the compression error in the first place that contributes to the total error, which is nevertheless still small enough for quantitative results.

Table 1: Runtimes for approximate and full MPSSI calculations with intermediate and final MPS compression to  $m = 500$  and  $2000$ , as run on 24 cores of an AMD EPYC 7502 CPU.

$m$	approx.	full
500	6h 2m	21h 46m
2000	2d 3h	15d 19h

Table 1 discloses the massive speedup that both the MPSSI approximation and the compression entail. Compared to a full MPSSI calculation with  $m = 2000$ , the MPSSI approximation gains a 7.5-fold speedup, the compression alone to  $m = 500$  gains a 18-fold speedup, and the combination of both methods gains an overwhelming 63-fold speedup. Both, the MPSSI approximation and compression are essentially able to eliminate the bottlenecks in the MPSSI method, while still retaining for quantitative accuracy.

Although the smallest  $m$  value of 500 chosen by us is dictated by the original  $m$  value employed during the wave function optimisation, it is tempting to use an even smaller value to save further computational time. However, given the comparably larger compression error that would increase even further for smaller  $m$  values, we do not recommend such a reduction.

## 4 Conclusion

In this work we presented two modifications to the original formulation of the MPSSI method by Knecht et al.<sup>23</sup>, which despite simple allow for drastic computational savings while retaining controlled accuracy in the DMRG-SCF calculation of properties.

The first modification, named the “MPSSI approximation”, is based on the omission of the quadratic term in the operator that is employed to counterrotate the MPS, to match the effect of the basis transformation. The second modification consist of decreasing the maximum bond dimension of the intermediate and the final counterrotated MPS by the SVD compression with a smaller  $m$  value. The accuracy of both modifications may be controlled independently of each other by a numerical parameter. In case of the MPSSI approximation, it is the  $L^2$  norm of the  $\mathbf{t} - \mathbf{I}_L$  matrix employed for the orbital rotation,

which is known before the time-consuming MPS counterrotation, and thus allows for an error estimate of the MPSSI approximation beforehand. For the MPS compression, it is the  $m$  value of the intermediate and the final compressed MPS.

We have tested both modifications in two common useful scenarios where efficiency is highly desired: the calculation of wavefunction overlaps and spin-orbit couplings. Both quantities are for example indispensable to perform efficient ab initio non-adiabatic simulations on-the-fly. In all our examples the discrepancies in these properties due to the MPSSI approximation error were very small. For tightly-converged DMRG-SCF wavefunctions, close enough to CASSCF wavefunctions, the MPSSI approximation error was found to be larger than the DMRG approximation error, but unlike the latter not dependent on the wavefunction quality. Instead, it shows monotonous dependence on the  $L^2$  norm of the  $\mathbf{t} - \mathbf{I}_L$  matrix. When DMRG-SCF employs large active spaces, the MPS compression to the original  $m$  value of the unrotated MPS allows for very substantial computational time savings but introduces an additional source of error: although the MPS compression error is larger than that of the MPSSI approximation, it is still small enough to allow quantitative computation of properties.

In the current calculations, the MPSSI approximation and the MPS compression to  $m = 500$  gave us a total 63-fold speedup compared to a calculation with compression to  $m = 2000$ , while maintaining a total error still small enough for quantitative computation of properties. The compression to  $m = 8000$  as in the original implementation could not be performed due to excessive computational requirements: the performance gain compared to such a calculation would have been even larger. We believe that the speedups achieved with the improvements in this work will pave the way to faster and more affordable large-scale multiconfigurational calculations, as well as allow DMRG-SCF to be applied in computationally intensive scenarios, e.g. in ab-initio excited state molecular dynamics simulations.

## Acknowledgements

L. F. thanks the Austrian Science Fund (FWF) for generous funding via the Schrödinger fellowship (project no. J 3935-N34). The University of Vienna is thanked for continuous support and the VSC for the computational resources.

## Author information

Leon Freitag: ORCID: **0000-0002-8302-1354**

Alberto Baiardi: ORCID: **0000-0001-9112-8664**

Stefan Knecht: ORCID: **0000-0001-9818-2372**

Leticia González: ORCID: **0000-0001-5112-794X**

## References

- (1) Szalay, P. G.; Müller, T.; Gidofalvi, G.; Lischka, H.; Shepard, R. Multiconfiguration Self-Consistent Field and Multireference Configuration Interaction Methods and Applications. *Chem. Rev.* **2012**, *112*, 108–181.
- (2) Roca-Sanjuán, D.; Aquilante, F.; Lindh, R. Multiconfiguration Second-Order Perturbation Theory Approach to Strong Electron Correlation in Chemistry and Photochemistry. *WIREs Comput. Mol. Sci.* **2012**, *2*, 585–603.
- (3) Olsen, J. The CASSCF Method: A Perspective and Commentary. *Int. J. Quantum Chem.* **2011**, *111*, 3267–3272.
- (4) Vogiatzis, K. D.; Ma, D.; Olsen, J.; Gagliardi, L.; de Jong, W. A. Pushing Configuration-Interaction to the Limit: Towards Massively Parallel MCSCF Calculations. *J. Chem. Phys.* **2017**, *147*, 184111.

- (5) Aquilante, F.; Autschbach, J.; Carlson, R. K.; Chibotaru, L. F.; Delcey, M. G.; De Vico, L.; Fdez. Galván, I.; Ferré, N.; Frutos, L. M.; Gagliardi, L.; Garavelli, M.; Giussani, A.; Hoyer, C. E.; Li Manni, G.; Lischka, H.; Ma, D.; Malmqvist, P. A. k.; Müller, T.; Nenov, A.; Olivucci, M.; Pedersen, T. B.; Peng, D.; Plasser, F.; Pritchard, B.; Reiher, M.; Rivalta, I.; Schapiro, I.; Segarra-Martí, J.; Stenrup, M.; Truhlar, D. G.; Ungur, L.; Valentini, A.; Vancoillie, S.; Veryazov, V.; Vysotskiy, V. P.; Weingart, O.; Zapata, F.; Lindh, R. Molcas 8: New Capabilities for Multiconfigurational Quantum Chemical Calculations across the Periodic Table. *J. Comput. Chem.* **2016**, *37*, 506–541.
- (6) White, S. R. Density Matrix Formulation for Quantum Renormalization Groups. *Phys. Rev. Lett.* **1992**, *69*, 2863–2866.
- (7) White, S. R. Density-Matrix Algorithms for Quantum Renormalization Groups. *Phys. Rev. B* **1993**, *48*, 10345–10356.
- (8) White, S. R.; Martin, R. L. Ab Initio Quantum Chemistry Using the Density Matrix Renormalization Group. *J. Chem. Phys.* **1999**, *110*, 4127–4130.
- (9) Mitrushenkov, A. O.; Fano, G.; Ortolani, F.; Linguerri, R.; Palmieri, P. Quantum Chemistry Using the Density Matrix Renormalization Group. *J. Chem. Phys.* **2001**, *115*, 6815–6821.
- (10) Mitrushenkov, A. O.; Linguerri, R.; Palmieri, P.; Fano, G. Quantum Chemistry Using the Density Matrix Renormalization Group II. *J. Chem. Phys.* **2003**, *119*, 4148–4158.
- (11) Mitrushchenkov, A. O.; Fano, G.; Linguerri, R.; Palmieri, P. On the Importance of Orbital Localization in QC-DMRG Calculations. *Int. J. Quantum Chem.* **2011**, *112*, 1606–1619.
- (12) Chan, G. K.-L.; Zgid, D. In *Annual Reports in Computational Chemistry*; Wheeler, R. A., Ed.; Elsevier, 2009; Vol. 5; pp 149–162.

- (13) Marti, K. H.; Reiher, M. The Density Matrix Renormalization Group Algorithm in Quantum Chemistry. *Z. Phys. Chem.* **2010**, *224*, 583–599.
- (14) Wouters, S.; Van Neck, D. The Density Matrix Renormalization Group for Ab Initio Quantum Chemistry. *Eur. Phys. J. D* **2014**, *68*, 272.
- (15) Baiardi, A.; Reiher, M. The Density Matrix Renormalization Group in Chemistry and Molecular Physics: Recent Developments and New Challenges. *J. Chem. Phys.* **2020**, *152*, 040903.
- (16) Freitag, L.; Reiher, M. In *Quantum Chemistry and Dynamics of Excited States: Methods and Applications*; González, L., Lindh, R., Eds.; Wiley, 2020; Vol. 1; pp 207–246.
- (17) Zgid, D.; Nooijen, M. The Density Matrix Renormalization Group Self-Consistent Field Method: Orbital Optimization with the Density Matrix Renormalization Group Method in the Active Space. *J. Chem. Phys.* **2008**, *128*, 144116.
- (18) Zgid, D.; Nooijen, M. Obtaining the Two-Body Density Matrix in the Density Matrix Renormalization Group Method. *J. Chem. Phys.* **2008**, *128*, 144115.
- (19) Malmqvist, P.-A.; Roos, B. O. The CASSCF State Interaction Method. *Chem. Phys. Lett.* **1989**, *155*, 189–194.
- (20) Malmqvist, P. A. Calculation of Transition Density Matrices by Nonunitary Orbital Transformations. *Int. J. Quantum Chem.* **1986**, *30*, 479–494.
- (21) Olsen, J.; Godefroid, M. R.; Jönsson, P.; Malmqvist, P. A.; Fischer, C. F. Transition Probability Calculations for Atoms Using Nonorthogonal Orbitals. *Phys. Rev. E* **1995**, *52*, 4499–4508.
- (22) Malmqvist, P. A.; Rendell, A.; Roos, B. O. The Restricted Active Space Self-Consistent-Field Method, Implemented with a Split Graph Unitary Group Approach. *J. Phys. Chem.* **1990**, *94*, 5477–5482.

- (23) Knecht, S.; Keller, S.; Autschbach, J.; Reiher, M. A Nonorthogonal State-Interaction Approach for Matrix Product State Wave Functions. *J. Chem. Theory Comput.* **2016**, *12*, 5881–5894.
- (24) Roemelt, M. Spin Orbit Coupling for Molecular Ab Initio Density Matrix Renormalization Group Calculations: Application to g-Tensors. *J. Chem. Phys.* **2015**, *143*, 044112.
- (25) Sayfutyarova, E. R.; Chan, G. K.-L. A State Interaction Spin-Orbit Coupling Density Matrix Renormalization Group Method. *J. Chem. Phys.* **2016**, *144*, 234301.
- (26) Sayfutyarova, E. R.; Chan, G. K.-L. Electron Paramagnetic Resonance G-Tensors from State Interaction Spin-Orbit Coupling Density Matrix Renormalization Group. *J. Chem. Phys.* **2018**, *148*, 184103.
- (27) Knecht, S.; Legeza, O.; Reiher, M. Communication: Four-Component Density Matrix Renormalization Group. *J. Chem. Phys.* **2014**, *140*, 041101.
- (28) Battaglia, S.; Keller, S.; Knecht, S. An efficient relativistic density-matrix renormalization group implementation in a matrix-product operator formulation. *J. Chem. Theory Comput.* **2018**, *14*, 2353–2369.
- (29) Crespo-Otero, R.; Barbatti, M. Recent Advances and Perspectives on Nonadiabatic Mixed Quantum–Classical Dynamics. *Chem. Rev.* **2018**, *118*, 7026–7068.
- (30) Lengsfeld III, B. H.; Saxe, P.; Yarkony, D. R. On the Evaluation of Nonadiabatic Coupling Matrix Elements Using SA-MCSCF/CI Wave Functions and Analytic Gradient Methods. I. *J. Chem. Phys.* **1984**, *81*, 4549–4553.
- (31) Stålring, J.; Bernhardsson, A.; Lindh, R. Analytical Gradients of a State Average MCSCF State and a State Average Diagnostic. *Mol. Phys.* **2001**, *99*, 103–114.
- (32) Snyder, J. W.; Hohenstein, E. G.; Luehr, N.; Martínez, T. J. An Atomic Orbital-Based Formulation of Analytical Gradients and Nonadiabatic Coupling Vector Elements for

- the State-Averaged Complete Active Space Self-Consistent Field Method on Graphical Processing Units. *J. Chem. Phys.* **2015**, *143*, 154107.
- (33) Snyder, J. W.; Fales, B. S.; Hohenstein, E. G.; Levine, B. G.; Martínez, T. J. A Direct-Compatible Formulation of the Coupled Perturbed Complete Active Space Self-Consistent Field Equations on Graphical Processing Units. *J. Chem. Phys.* **2017**, *146*, 174113.
- (34) Mai, S.; Marquetand, P.; González, L. Nonadiabatic Dynamics: The SHARC Approach. *WIREs Comput. Mol. Sci.* **2018**, *8*, e1370.
- (35) Granucci, G.; Persico, M.; Toniolo, A. Direct Semiclassical Simulation of Photochemical Processes with Semiempirical Wave Functions. *J. Chem. Phys.* **2001**, *114*, 10608–10615.
- (36) Freitag, L.; Ma, Y.; Baiardi, A.; Knecht, S.; Reiher, M. Approximate Analytical Gradients and Nonadiabatic Couplings for the State-Average Density Matrix Renormalization Group Self-Consistent-Field Method. *J. Chem. Theory Comput.* **2019**, *15*, 6724–6737.
- (37) Schollwöck, U. The Density-Matrix Renormalization Group in the Age of Matrix Product States. *Ann. Phys.* **2011**, *326*, 96–192.
- (38) Schollwöck, U. The Density-Matrix Renormalization Group: A Short Introduction. *Phil. Trans. R. Soc. A* **2011**, *369*, 2643–2661.
- (39) Keller, S.; Dolfi, M.; Troyer, M.; Reiher, M. An Efficient Matrix Product Operator Representation of the Quantum Chemical Hamiltonian. *J. Chem. Phys.* **2015**, *143*, 244118.
- (40) Ronconi, L.; Sadler, P. J. Photoreaction Pathways for the Anticancer Complex Trans,Trans,Trans-[Pt(N<sub>3</sub>)<sub>2</sub>(OH)<sub>2</sub>(NH<sub>3</sub>)<sub>2</sub>]. *Dalton Trans.* **2011**, *40*, 262–268.

- (41) Bednarski, P. J.; Korpis, K.; Westendorf, A. F.; Perfahl, S.; Grünert, R. Effects of Light-Activated Diazido-Pt<sup>IV</sup> Complexes on Cancer Cells in Vitro. *Phil. Trans. R. Soc. A* **2013**, *371*, 20120118.
- (42) Shi, H.; Imberti, C.; Sadler, P. J. Diazido Platinum(IV) Complexes for Photoactivated Anticancer Chemotherapy. *Inorg. Chem. Front.* **2019**, *6*, 1623–1638.
- (43) Freitag, L.; González, L. The Role of Triplet States in the Photodissociation of a Platinum Azide Complex by a Density Matrix Renormalization Group Method. *J. Phys. Chem. Lett.* **2021**, *12*, 4876–4881.
- (44) Hammes-Schiffer, S.; Tully, J. C. Proton Transfer in Solution: Molecular Dynamics with Quantum Transitions. *J. Chem. Phys.* **1994**, *101*, 4657.
- (45) Plasser, F.; Granucci, G.; Pittner, J.; Barbatti, M.; Persico, M.; Lischka, H. Surface Hopping Dynamics Using a Locally Diabatic Formalism: Charge Transfer in the Ethylene Dimer Cation and Excited State Dynamics in the 2-Pyridone Dimer. *J. Chem. Phys.* **2012**, *137*, 22A514.
- (46) Plasser, F.; Ruckebauer, M.; Mai, S.; Oppel, M.; Marquetand, P.; González, L. Efficient and Flexible Computation of Many-Electron Wavefunction Overlaps. *J. Chem. Theory Comput.* **2016**, *12*, 1207–1219.
- (47) Plasser, F.; González, L. Communication: Unambiguous Comparison of Many-Electron Wavefunctions through Their Overlaps. *J. Chem. Phys.* **2016**, *145*, 021103.